Electronic structure and origin of visible-light activity of C-doped cubic In_2O_3 from first-principles calculations

Run Long, Niall J. English*

The SEC Strategic Research Cluster and the Centre for Synthesis and Chemical Biology, School of Chemical and Bioprocess Engineering, University College Dublin, Belfield, Dublin 4, Ireland

Abstract: The origin of the experimentally observed band gap narrowing and red-shift of the adsorption edge of cubic In_2O_3 induced by C doping has been investigated using density functional theory calculations. We have compared the stability of all these doped systems based on the calculated formation energy as a function of the oxygen chemical potential. The calculated electronic structures show that: (I) at low C concentration, substitutional replacement of O by C could lead to small gap narrowing, owing to C 2p states below the conduction band minimum while interstitial C doping does not induce band gap narrowing; and (II) at high C concentration, C2p states mix well with O 2p states above the valence band, which may account for the experimentally observed red-shift of the absorption edge.

Abstract: C-doped In_2O_3, C doping concentration, band structure, red-shift

* Corresponding author. E-mail: niall.english@ucd.ie; Tel.: +353-1-7161646; Fax: +353-1-7161177

1. Introduction

Photocatalysts have received much attention since the photoinduced decomposition of water on TiO_2 electrodes by Honda and Fujishima in 1972 [1]. However, its widespread application has been restricted to ultraviolet light ($\lambda < 385$ nm) due to its wide band gap (~3.2 eV for anatase and 3.0 eV for rutile). To shift the absorption edge to the visible light region, much experimental and theoretical activity to specify and fabricate such photocatalysts has been reported, *e.g.*, by anionic or cationic impurity doping [2, 3, 4], dye sensitization, and in combination with smaller band gap semiconductor [5, 6]. However, there exist typically some drawbacks in TiO_2-based photocatalysts, such as the large formation energy required by impurity doping, fast electron-hole recombination, and small gap narrowing. Recently, codoping of transition metal and non-metal elements into TiO_2 has attracted much attention and shown much more efficiency than monodoping under visible-light irradiation [7-10]. The search for new efficient visible light photocatalysts other than titania has been attempted experimentally and it appears that the class of materials formally having d^{10} electronic configurations (In^{3+}, Ga^{3+}, Ge^{4+}, Sn^{4+}, and Sb^{5+}) are good potential candidates because the electronic configurations of d^0 (Ti^{4+}) and d^{10} are similar in their absence of *d* electron participation in photoexciation, which appears to be an important key to their photocatalytic activity [11]. Recently, Sun et al. [12] reported that C-doped cubic In_2O_3 showed increased absorption in the 350-500 nm range with a red-shift in the band gap transition and higher photocatalytic activity under visible light irradiation; it was also shown that the high C doping concentration could lead to large photocurrents. As expected, C dopant concentration should also have a large

influence on the electronic structure of C-doped In_2O_3. Although C-doped TiO_2 has been systemically investigated both in experiment and theory, the nature of C-induced modifications of the TiO_2 electronic band structure is still controversial. Either band gap narrowing [13] or the formation of localized midgap states [14] have been proposed to account for the red-shift of the optical absorption edge; dopant sites, either substitutional or interstitial, can lead to different gap-narrowing mechanisms. On the basis of X-ray photoelectron spectroscopy (XPS), Sun et al. [12] suggested that carbonate species dominate the impurity structure in C-doped In_2O_3 samples and indicated that further NMR experiments are needed to identify the dopant structure more fully in C-doped In_2O_3. Thus, the most basic question about the character of carbon impurities, *i.e.*, whether carbon is substitutional or interstitial when introduced into an In_2O_3 matrix, need to be investigated theoretically in the absence of enough experimental results. In addition, to the best of our knowledge, there is little theoretical work on C-doped In_2O_3 to clarify the microelectronic mechanisms of the origin of gap narrowing, as well as the influence of C doping concentration on modifications in electronic structure.

To address these questions, in the present study, we investigate the effect of both substitutional and interstitial C-doping on the structural and electronic properties of cubic In_2O_3, using density functional theory (DFT) calculations. The stability of all of these doping species has been compared based on calculated formation energies. To obtain insights into C-induced modifications of the In_2O_3 electronic band structure, we have performed a careful analysis of the C impurity states and their influence on the In_2O_3 band structure with low and high C doping concentration. Our results

rationalize the experimentally reported red-shift of the optical absorption edge [12].

2. Methodology

The stable phase of In_2O_3 (cf. Fig. 1a) adopts the body-centered cubic bixbyite ($FeMnO_3$) structure (space group $Ia\bar{3}$) with 8 fundamental units per primitive cell [15]. Each In atom is coordinated by six oxygen atoms in a distorted octahedron, with O-In bond lengths ranging from 2.13-2.23 Å and a lattice parameter of 10.117 Å [15]. Substitutional C doping was modeled by replacing one O atom by one C ($C_{s\text{-}O}$) in the 80-atom In_2O_3 supercell. Interstitial doping (C_i) was modeled by adding one C atom into the pure In_2O_3 supercell. To take into account of the doping concentration, another two or three C dopants was substituted for the same number of oxygen atoms in C-doped In_2O_3, namely $C_{2s\text{-}O}$ and $C_{3s\text{-}O}$.

All of the spin-polarized calculations were performed using the projector augmented wave (PAW) pseudopotentials as implemented in the VASP code [16, 17]. The Perdew-Burke-Ernzerhof parametrization [18] of generalized gradient approximation [19] is adopted for the exchange-correlation potential. The electron wave function was expanded in plane waves up to a cutoff energy 400 eV and Monkhorst–Pack *k*-point mesh [20] of 2 × 2 × 2 was used for geometry optimization and a higher *k*-point mesh 4 × 4 × 4 for calculation of the density of states. Both the cell and atomic relaxations were carried out until the residual forces were below 0.01 eV/Å. The optimized lattice parameter is 10.211Å, in good agreement with the experimental value of 10.117 Å [15] (error less than 0.9%).

3. Results and Discussion

3.1 Optimized Structures and Formation energy

The optimized local structures of $C_{s\text{-}O}$, and C_i are shown in Figs. 1(b)-1(c). For the $C_{s\text{-}O}$ model (cf. Fig. 1 (b)), two C-In bonds and one C-O bond were performed. The relaxed C–In bond lengths are 2.451, and 2.458 Å, and the optimized C-O bond length is 1.225 Å: a large lattice distortion is induced due to the large differences in ion radius between the C and O atom. For example, the optimized O-In bond lengths are 2.146, 2.216, and 2.241 Å in pure In_2O_3. In addition, the 1.225 Å distance of C-O is very close to the C=O double bond length of 1.20 Å in a CO_2 molecule. It was expected that there exists a relatively weak ionic bond between the C atoms and adjacent In atoms, while a strong C-O covalent bond was formed. For C_i doping, two C-In bonds are formed and one C-O bond, with lengths of 2.415, 2.362, and 1.211 Å, respectively, as shown in Fig. 1(c). Surprisingly, all of the C-O distances approximate each other between $C_{s\text{-}O}$ and C_i doping at around 1.20 Å, and suggests the presence of carbonate species, agreeing well with experimental findings [12].

To study the variation of chemical bonding induced by C atoms, we calculated the total charge densities for $C_{s\text{-}O}$, C_i, and C_i modes, and they are shown in Fig. 2. In the case of $C_{s\text{-}O}$ model (cf. Fig. 2 a), the C dopant and two adjacent In atoms and one O atom form C-In bonds and a C-O bond through charge transfer after electron redistribution. It is shown clearly that ionic bonding behavior dominates the C-In bond while the C-O bond displays mainly covalent character. Furthermore, the calculated Bader charge [21] shows the C dopant is in a positive oxidation state and its charge is increased to about 0.98|e| because many more electrons are trapped by its

adjacent O atom than by trapped electrons from adjacent In atoms owing to electronegativities in the order O (3.44) > C (2.55) > In (1.78) [22]. Here, the total charge of CO species is about -1.04|e|, which indicates that CO^{2-} may exist as a paramagnetic species in the lattice and agrees well with the C-O distance of 1.225 Å. It was found that a single O replacement by one C induces a magnetic moment of 2.0 μ_B in our calculation. The calculated spin density is shown in Fig.2 b and indicates that spin density is centered primarily on the N atoms and its adjacent O atoms.

For C_i doping (Fig. 2c), the C atom is tightly bound with the adjacent O atom and interacts weakly with two adjacent In atoms, showing C-O covalent bonding behavior and C-In ionic bonding character, respectively. The Bader charge on CO^{2-} species is -0.64|e|. The bonding characteristics are very similar to $C_{s\text{-}O}$ doping, which is reasonable given the similar C-In and C-O bond lengths in these two cases. At the same time, the spin density distribution (cf. Fig. 2 d) is also similar to $C_{s\text{-}O}$ doping. Therefore, both of the models form CO^{2-} species, consistent with results for C-O bond lengths. This is supported by findings from XPS experiments and SSNMR measurements, which reported that existence of only carbonate species in C-doped In_2O_3 samples [12].

It is necessary to clarify as to whether the C dopant would exist as a substitutional or interstitial impurity in the lattice. To evaluate the relative difficulty for the incorporation of C dopants into host lattice, the formation energies were calculated based on the oxygen chemical potential, which can also determine the relative stability of the doped systems. The formation energies of $C_{s\text{-}O}$, and C_i can be calculated according to the formulae

$$E_{form} = E(doped) - E(pure) - \mu_C + \mu_O \quad (1)$$

$$E_{form} = E(doped) - E(pure) - \mu_C \quad (2)$$

where $E(doped)$ and $E(pure)$ are the total energies of the In_2O_3 supercell with and without the C dopant, respectively. The formation energies for the different doped systems were considered in this work as a function of the oxygen chemical potential (μ_O), which is a parameter that characterizes the oxygen environment during synthesis [23, 24]. The environment acts as a reservoir, which can give or take any amount of oxygen without changing its temperature and pressure [25]. Low and high values of μ_O correspond to O-poor and -rich conditions, respectively. By referencing μ_O to the energy of an O atom in an O_2 molecule ($\mu_O = \frac{1}{2}\mu(O_2) + \mu_O^{'}$), we take $-4.4eV \le \mu_O^{'} \le 0eV$, where the value $\mu_O^{'} = 0$ corresponds to the O-rich limit, whereas $\mu_O^{'}$ = -4.4 eV is approximately half the enthalpy of formation of cubic In_2O_3 (the experimental value for which is 9.60 eV) [22]. The chemical potential for C (μ_C), was fixed and calculated from the formula $\mu_C = \mu_{CO_2} - \mu_{O_2}$. The calculated formation energies for $C_{s\text{-}O}$, and C_i doping are summarized in Table 1. It should be noted that the values of the formation energies vary between the O-rich and -poor growth conditions. The behavior may be summarized as follows: 1) E_{form} increases with μ_O, indicating O-poor conditions are more favorable for the replacement of host O atoms by C atoms; 2) conversely, the replacement of one host O atom by a C atom has large formation energy under O-rich growth conditions; 3) the formation energy of C_i shows essentially no dependence on μ_O, with an intermediate value. Generally, O-rich growth conditions are the case in sol-gel methods to synthesize In_2O_3 samples experimentally. From our results, small differences in the formation energy indicate

that substitutional O and interstitial C are energetically viable in real materials.

3.2 Electronic Structures

3.2.1 Pure In_2O_3

To investigate how to modify the band gap of In_2O_3 via doping, a knowledge of the characteristics of the band edges in pure In_2O_3 is needed. The band structure and projected density of states (PDOS) are plotted in Figure 3. The calculated band gap of pure In_2O_3 is 1.1 eV, closing to the calculated value of 0.8 eV by the DFT +U method of Walsh et al [26] owing to absence of d orbitals in edge of conduction band and valence band, which is still a largely underestimate vis-à-vis the experimental band gap of 3.0-3.5 eV [27-30]. However, we are primarily interested in trends of variation in the band gap, and only the relative positions of the occupied states and empty states need to be considered. In particular, the conduction band (CB) edge at the Gamma (G) point is well dispersed, which could serve to prohibit the recombination of electrons and holes through this band. This explains the relatively high observed electronic conductivity of In_2O_3. The PDOS shows that the valence band (VB) edge are flat and are dominated by O 2p states while the CB edge originates from the In 5s states. This indicates that the electron transition from O 2p to In 5s states is responsible for onset of optical absorption. Therefore, it is expected that the C dopant will either result in band gap narrowing or induce localized states in the gap, similar to C-doped TiO_2 [24].

3.2.2 C- doped In_2O_3

To investigate the influence of N dopant on the modification of the band gap, we have calculated the band structure and shown this in Figure 4. Fig. 4a depicts clearly band gap narrowing is tiny for $C_{s\text{-}O}$ doping with a value of about 0.1 eV (see spin-up) compared to the pure case. On the other hand, there is almost no change of the band gap for C_i doping with respect to pure In_2O_3. This behavior is very different from C-doped TiO_2 [24]. To explore further the effect C doping on the modification of electronic structure, the density of states (DOS) and PDOS were calculated and are plotted in Figure 5, along with pure In_2O_3 (cf. Figs. 5a&a'). For $C_{s\text{-}O}$ doping (cf. Figs. 5b&b'), there are no C 2p states mixed with O 2p states near the edge of valence band and no isolated C 2p states above the valence band maximum (VBM). However, there are some C 2p states just below the host conduction band minimum (CBM), although most of them reside in the conduction band, which could be responsible for the red-shift of C-doped TiO_2 reported in experiment [12]. For For C_i doping (cf. Figs. 5c&c'), the C 2p states locate mostly in the conduction band and do not contribute to the edge of either the conduction or valence band. Therefore, the band gap for C_i doping changes little vis-à-vis the pure case. As mentioned above, this behavior is markedly different from C-doped TiO_2 in (both interstitial and replacement for O) [24]. Therefore, at this low C doping concentration, band gap narrowing is not obvious.

To investigate the influence of higher C doping concentration on the electronic structure of substitutionally C-doped In_2O_3, the calculated DOS and PDOS are shown in Fig. 6 for two- and three-atom replacement. Both of these cases exhibit significant gap narrowing and that C 2p states mix well with O 2p states near the edge of the valence band, which could be responsible for the obvious red-shift of the absorption edge. The gap narrowing mechanism is obvious different from the low C-doped In_2O_3.

4. Conclusions

We have studied the structural and electronic properties of C-doped In_2O_3 by

density functional theory calculations based on the plane-wave method. The calculated formation energy results indicate that substitutional and interstitial C doping has similar values under O-rich growth conditions, which is the sol-gel experimental synthesis condition. At the low C concentration, C replacement of an O atom induces a few C 2p gap states close to the bottom of the conduction band, which may account for the experimentally observed red-shift of absorption. At high C concentration, substitutional C-doping leads to band gap narrowing due to C 2p gap states mixing well with O 2p states above the valence band. On the other hand, interstitial C doping does not induce band gap narrowing. These results serve to rationalize experimental observations of increased photoactivity [12].

References

(1) Fujishima, A.; Honda, K. *Nature* **1972**, *28*, 37.

(2) Karakitsou, K. E.; Verkios, X. E. *J. Phys. Chem*. **1993**, *97*, 1184.

(3) Sakthivel, S. Kisch, T.; *Angew Chem. Int. Ed*. **2003**, *32*, 772.

(4) Yang, K. S.; Dai, Y.; Huang, B. B.; and Han, S. H. *J. Phys. Chem. B* **2006**, *110*, 24011.

(5) Duncan, W. R.; Prezhdo, O. V. *J. Am. Chem. Soc*. **2008**, *130*, 9756.

(6) Lin, J.; Yu, J. C.; Lo, D.; Lam. S. K. *J. Cata*. **1999**, *183*, 368.

(7) Shen, Y. F.; Xiong, T. Y.; Li, T. F.; Yang, K. *Appl. Catal., B* **2008**, *83*,177.

(8) Long, R.; English, N. J. *Chem. Mater.* **2010**, *22*, 1616.

(9) Long, R.; English, N. J. *Chem. Phys. Lett.* **2009**, *478*, 175.

(10) Gai, Y. Q.; Li, J. B.; Li, A. S.; Xia, J. B.; Wei, S. H. *Phys. Rev. Lett.* **2009**, *102*, 036402.

(11) Inoue, Y. *Chem. Ind.* **2006**, *108*, 623.

(12) Yan, P. S.; Carl, J. M.; Karla, R. R. G.; Enrique, A. R. G.; Justin P. L.; Daniel R. *Int. J. Hydrogen Energy* **2008**, *33*, 5967-5964.

(13) Barborini, E.; M.Conti, A.; Kholmanov, I. N.; Miseri, P.; Podestå, A.; Milani, P.; Cepek, C.; Sakho, O.; Macovez, R. Sancrotti, M. *Adv. Mater.* **2005**, *17*, 1842.

(14) Lee, J. Y.; Park, J.; Cho, J. H. *Appl. Phys. Lett.* **2005**, *87*, 011904.

(15) Bartos, A.; Lieb, K. P.; Uhrmacher, M.; Wiarda, D. *Acta Crystallogr. B* **1993**, *49*, 165.

(16) Kresse, G.; Hafner, J. *Phys. Rev. B* **1993**, *47*, RC558.

(17) Kresse, G.; Furtherműller, J. *Phys. Rev. B* **1996**, *54*, 11169.

(18) Perdew, J. P.; Burk, K.; and Ernzerhof, M. *Phys. Rev. Lett.* **1996**, *77*, 3865.

(19) Perdew, J. P.; and Wang, Y. *Phys. Rev. B* **1992**, *45*, 13244.

(20) Monkhorst, H. J.; Pack, J. D. *Phys. Rev. B* **1976**, *13*, 5188.

(21) Henkelman, G.; Arnaldsson, A.; and Jónsson, H. *Comput. Mater. Sci.* **2006**, *36*, 254.

(22) *CRC Handbook of Chemistry and Physics* 87th ed.; Lide, D. R. Taylor & Francis: London, 2006.

(23) Wilson, N. C.; Grey, I. E.; Russo, S. P. *J. Phys. Chem.C* **2007**, *111*,10915.

(24) (a) Valentin, C. Di.; Pacchioni, G.; Selloni, A. *Chem. Mater*. **2005**, *17*, 6656. (b) Graciani, J.; Ortega, Y.; and Sanz, F. *Chem. Mater.* **2009,** *21*, 1431.

(25) Reuter, K.; Scheffler, M. *Phys. Rev. B* **2001**, *65*, 035406.

(26) Walsh A.; Da Silva, J. L. F.; Wei, S. H.; Köber C.; Klein, A.; Piper, L. J. F.; DeMasi, A.; Smith, K. E.; Panaccione, G.; Torelli, P.; Payne, D. J.; Bourlange, A.; and Egdell R. G. *Phys. Rev. Lett.* **2008**, *100*, 167402.

(27) Hamberg, I.; Granquist, C. G.; Berggren, K. F.; Senelius, B. E.; Engstrom, L. *Phys. Re*V. *B* **1984**, *30*, 3240.

(28) King, P. D. C.; Veal, T. D.; Fuchs, F.; Wang, Ch. Y.; Payne, D. J.; Bourlange, A.; Zhang, H.; Bell, G. R.; Cimalla, V.; Ambacher, O.; Egdell, R. G.; Bechstedt, F.; MaConville, C. F. *Phys. Re*V. *B* **2009**, *79*, 205211.

(29) Weiher, R. L.; Ley, R. P. *J. Appl. Phys.* **1966**, *37*, 299.

(30) Matino, F.; Persano, L.; Arima, V.; Pisignano, D.; Blyth, R. I. R.; Cingolani, R.; Rinaldi, R. *Phys. Re*V. *B* **2005**, *72*, 085437.

Table 1. Calculated formation energies E_{form} (eV) for C-doped In_2O_3 systems.

E_{form} (eV)	O-rich	In-rich
$C_{s\text{-}O}$	*8.96*	*5.4*
C_i	*8.34*	*8.34*

Figure captions

Figure 1. (a) Optimized In_2O_3 supercell and optimized local geometries for (b) $C_{s\text{-}O}$ doping, and (c) C_i doping. The bond length unit is Å.

Figure 2. Band structure and projected density of states (PDOS) of pure cubic In_2O_3.

Figure 3 Total electron density maps (left panel) and spin density maps (right panel) for (a, b) $C_{s\text{-}O}$ and (c, d) C_i cases. The plot is in the plane of C-In and C-O bonds and their nearest-neighboring atoms (shown only on the plane for total electron density).

Figure 4 Band structure for (a) $C_{s\text{-}O}$ (top panel) and (b) C_i cases (bottom panel). The top of valence band of pure In_2O_3 is taken as the reference level.

Figure 5. Density of states (DOS) for (a) pure In_2O_3, (b) $C_{s\text{-}O}$ case, and (c) C_i doping. The corresponding PDOS are shown in (a')-(c'). The top of the valence band of pure In_2O_3 is taken as the reference level. The dashed lines represent the Fermi level E_F.

Figure 6. Density of states (DOS) for (a) $C_{2s\text{-}O}$- and (b) $C_{3s\text{-}O}$-doping. The corresponding PDOS are shown in (a') and (b'). The dashed lines represent the Fermi level E_F.

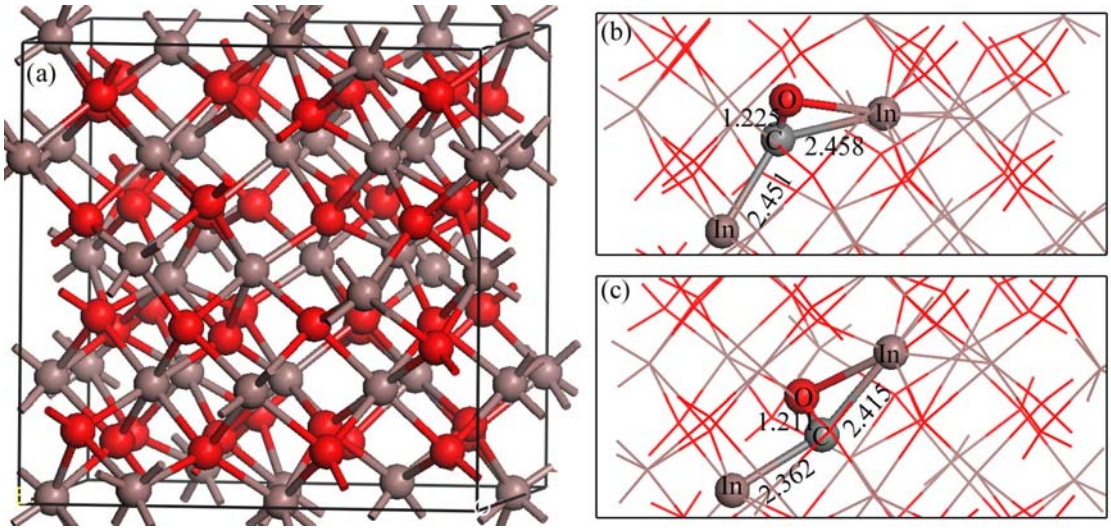

Figure 1

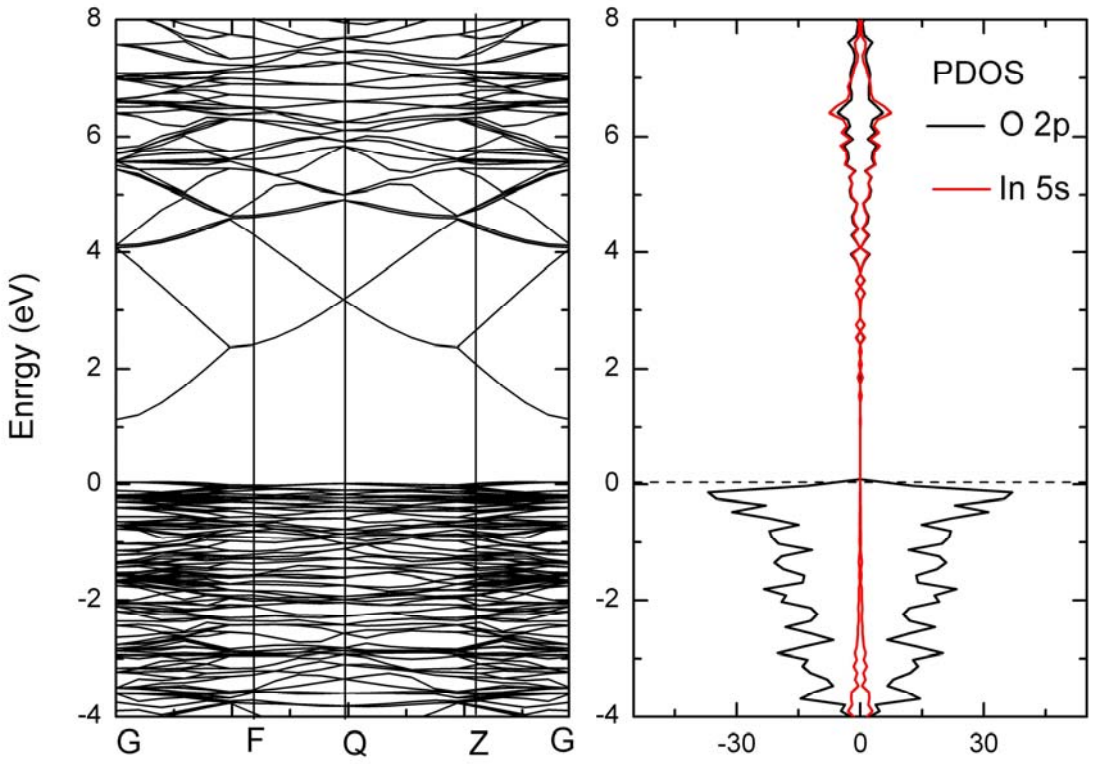

Figure 2

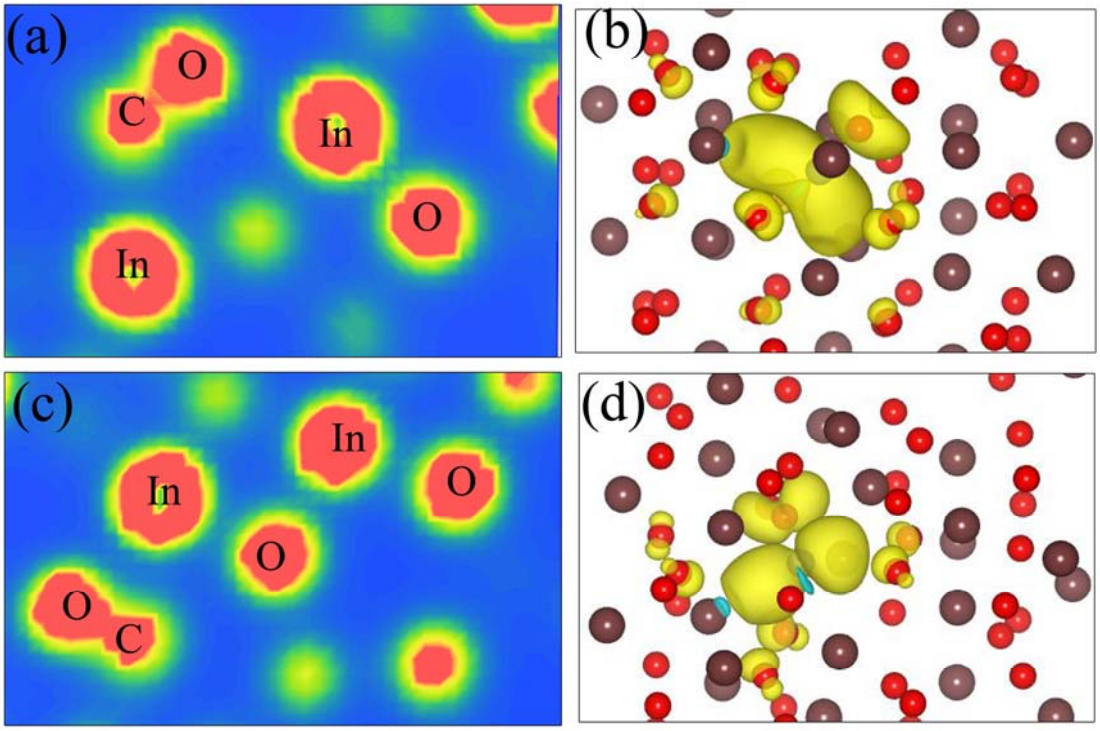

Figure 3

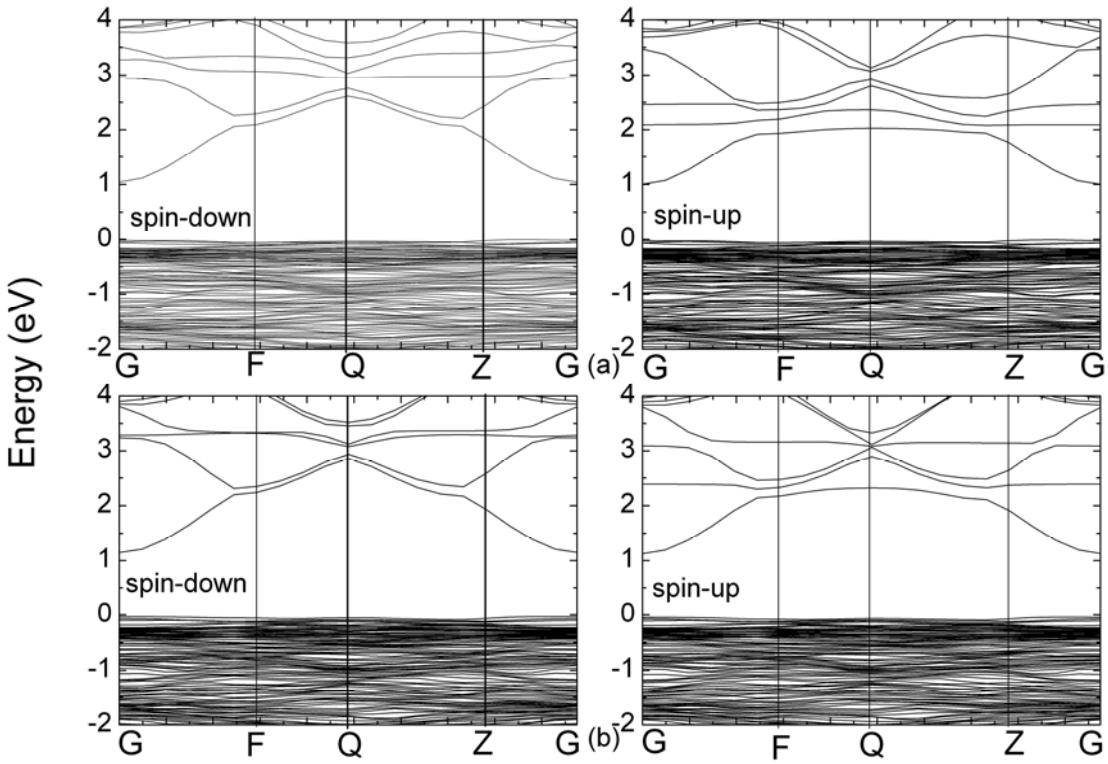

Figure 4

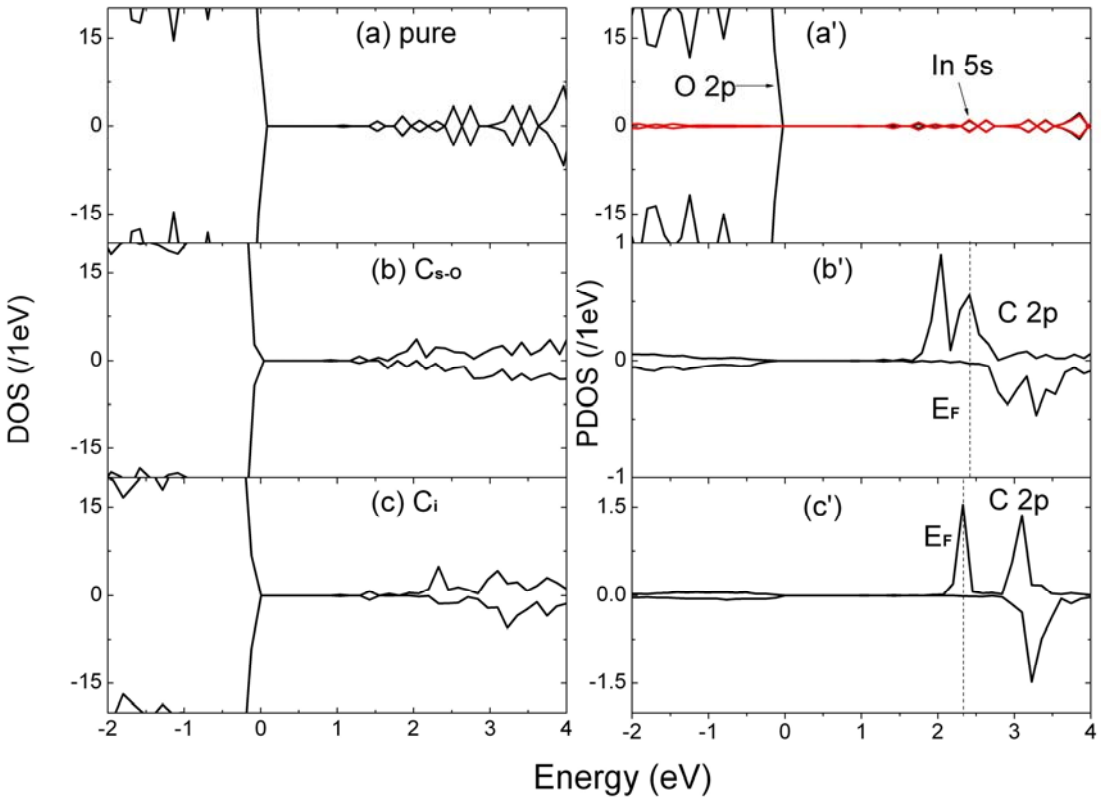
(a) pure
(b) C_{s-o}
(c) C_i
(a')
O 2p
In 5s
(b')
C 2p
E_F
(c')
C 2p
E_F
DOS (/1eV)
PDOS (/1eV)
Energy (eV)

Figure 5

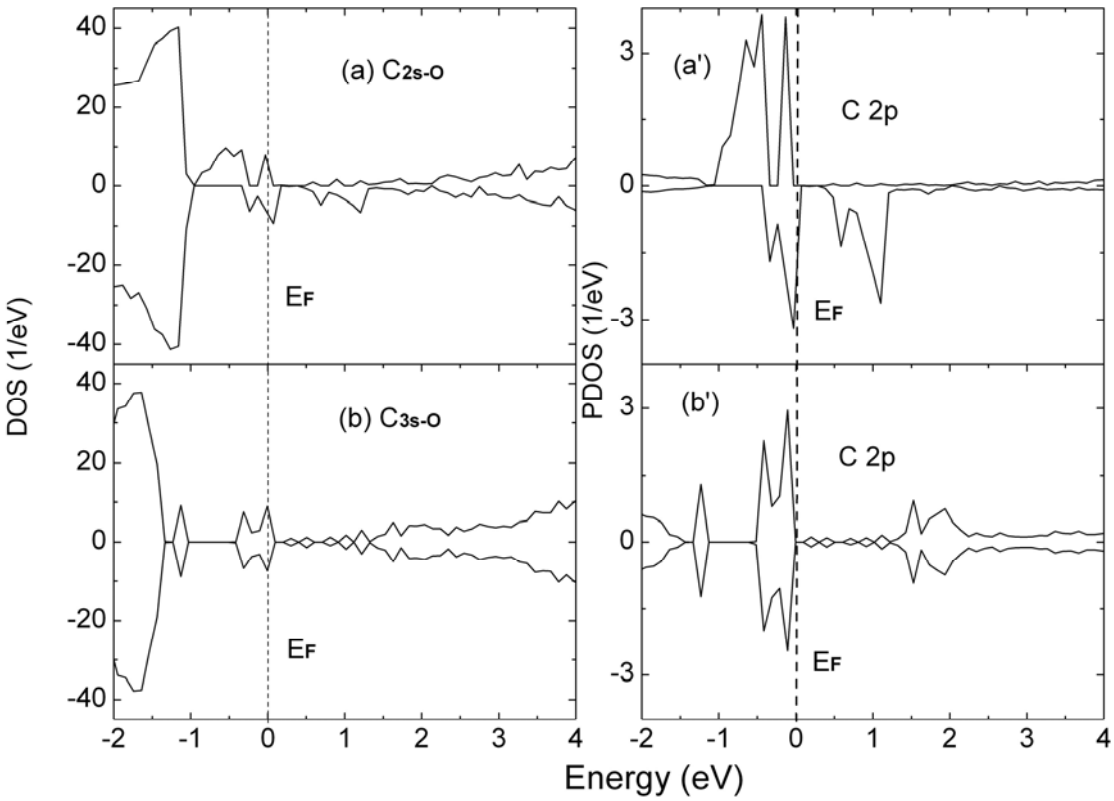

Figure 6